REPORT

NANOPHOTONICS

Probing the ultimate plasmon confinement limits with a van der Waals heterostructure

David Alcaraz Iranzo,[1]* Sébastien Nanot,[1,2]* Eduardo J. C. Dias,[3] Itai Epstein,[1] Cheng Peng,[4] Dmitri K. Efetov,[1,4] Mark B. Lundeberg,[1] Romain Parret,[1] Johann Osmond,[1] Jin-Yong Hong,[4] Jing Kong,[4] Dirk R. Englund,[4] Nuno M. R. Peres,[3] Frank H. L. Koppens[1,5]†

The ability to confine light into tiny spatial dimensions is important for applications such as microscopy, sensing, and nanoscale lasers. Although plasmons offer an appealing avenue to confine light, Landau damping in metals imposes a trade-off between optical field confinement and losses. We show that a graphene-insulator-metal heterostructure can overcome that trade-off, and demonstrate plasmon confinement down to the ultimate limit of the length scale of one atom. This is achieved through far-field excitation of plasmon modes squeezed into an atomically thin hexagonal boron nitride dielectric spacer between graphene and metal rods. A theoretical model that takes into account the nonlocal optical response of both graphene and metal is used to describe the results. These ultraconfined plasmonic modes, addressed with far-field light excitation, enable a route to new regimes of ultrastrong light-matter interactions.

Van der Waals heterostructrures are constructed by vertically stacking atomically thin materials, selected from a rich palette of thousands of materials such as graphene (semimetal), hexagonal boron nitride (h-BN, dielectric), and transition metal dichalcogenides (semiconductors) (*1*). These are key enablers for tailoring electronic, optical, and optoelectronic properties (*2*). The most common heterostructure for two-dimensional (2D) electronics is graphene encapsulated by h-BN, and recently, this system has also emerged as a platform for polaritonics (*3*, *4*), with the capability to strongly confine plasmon polaritons with a relatively long plasmon lifetime exceeding 500 fs at room temperature (*5*). Heterostructures of graphene, h-BN, and metals have revealed so-called propagating acoustic plasmons (*6*–*8*), in which metal screening confines the light in the space between the metal and the graphene, and it slows down the plasmon to a velocity almost as low as $c/300$ (with c the speed of light) (*9*). What is then the ultimate limit on the confinement of propagating or resonant plasmons? For bulk metal–based plasmonic systems such as tapers (*10*), grooves (*11*), metal-insulator-semiconductor (*12*), and metal-insulator-metal (*13*, *14*) waveguides, the confinement of propagating surface plasmon polaritons is limited by Landau damping (*15*). For example, the quality factor of plasmonic Fabry-Pérot modes dropped below one for a confinement below 15 nm (*14*). Further enhancement of optical fields to the nanometer scale is possible in hotspots (*16*–*18*), although these are broadband in character.

We present a graphene-insulator-metal platform that allows us to realize and probe the ultimate physical limits of (out-of-plane) confinement of propagating plasmons down to the ultimate physical boundary of a one-atom-thick layer (here, $\lambda_0/26{,}000$), and without sacrificing damping. We take advantage of the fact that plasmons in two-dimensional materials are fundamentally different from plasmons in bulk metals because the restoring force by the long-range Coulomb interactions, which are essential for the plasmon velocity and confinement, can be controlled by tailoring the external environment. For that reason, the out-of-plane confinement and wavelength compression can be increased strongly without suffering from Landau damping. We use far-field light to couple to these strongly confined plasmons and find a vertical mode length down to 0.3 nm, whereas higher-order Fabry-Pérot resonances reveal that the propagating character of the plasmons is preserved.

The basic device geometry consists of graphene as the plasmonic material, encapsulated by atomically thin dielectric materials (h-BN or Al_2O_3) and covered by a metallic rod array (Fig. 1A) [details on the fabrication processes are provided in (*19*)]. The advantages of the periodic metal-insulator-graphene system are twofold. First, the presence of the metal results in efficient screening of the graphene plasmons, squeezing the so-called screened graphene plasmons (SGPs) into the graphene-metal gap without reducing their lifetime. Although screening and coupling of radiation to plasmons in classical 2D electron gases (2DEGs) was previously achieved by using grating-gate field-effect-transistors in the terahertz range (*7*), a relatively thick barrier layer (~100 nm) prevented the confinement of plasmons to the subnanometer limit, as we report here. Second, metal rods facilitate efficient coupling between far-field light and the strongly confined plasmons, where the width of the rods defines the resonant conditions for the plasmon modes. This approach does not require patterning of the graphene into nanoribbons or nanodiscs such as for previous infrared graphene plasmonic studies with far-field light (*20*, *21*).

The effect of the coupling of far-field light into our devices is represented by the field profiles obtained with finite-difference time-domain (FDTD) simulations (Fig. 1, B and C). The plasmons are launched at the metal edges, and most of the electric field is confined between metal and graphene, with virtually no leakage into the metal. This confinement arises because the metal acts as a nearly perfect conductor that prevents most of the field penetration. Because image charges are induced in the metal, the plasmon mode is analogous to the antisymmetric plasmon mode of two nearby graphene sheets with twice the spacer thickness (*8*), known as acoustic plasmons, carrying larger momentum than for conventional plasmon resonances in graphene ribbons [(*19*), section 5.7]. Within the dielectric gap, the plasmons maintain their propagating character and reflect at the edges of the rod, forming what appears to be a standing wave pattern similar to two coupled Fabry-Pérot resonators (*22*).

Bringing the metal closer will increase the plasmon screening, which slows down the plasmons, as previously observed with scattering-type scanning near-field optical microscopy (*8*, *9*), and also enhances the vertical confinement, as shown for two different dielectric spacer materials and graphene conductivity models (local and nonlocal) (Fig. 1D). The most extreme case is that of a monolayer h-BN spacer, in which in theory the vertical plasmon confinement is below 1 nm. The calculated width of the resonance [(*19*), section 6] does not increase when reducing the spacer thickness s. Therefore, this platform allows us to access the ultimate confinement limits of propagating plasmons in two spatial directions: out-of-plane confinement defined by s and in-plane confinement governed by λ_0/λ_p.

The far-field approach presented above allows probing of this plasmon confinement by use of Fourier transform infrared (FTIR) transmission measurements. Gate-dependent, spectral extinction

[1]Institut de Ciències Fotòniques (ICFO)–The Institute of Photonic Sciences, The Barcelona Institute of Science and Technology, 08860 Castelldefels (Barcelona), Spain. [2]Laboratoire Charles Coulomb (L2C), Université de Montpellier, CNRS, 34095 Montpellier Cedex, France. [3]Centro de Física and Departamento de Física and QuantaLab, Universidade do Minho, P-4710-057 Braga, Portugal. [4]Department of Electrical Engineering and Computer Sciences, Massachusetts Institute of Technology, Cambridge, MA 02139, USA. [5]Institució Catalana de Recerca i Estudis Avançats (ICREA), Barcelona, Spain.
*These authors contributed equally to this work.
†Corresponding author. Email: frank.koppens@icfo.eu

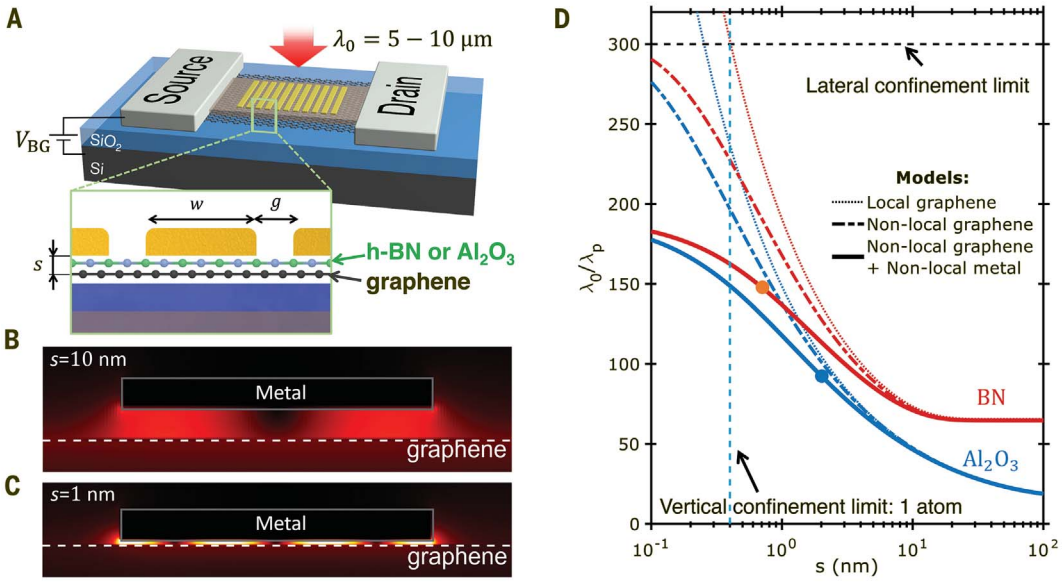

Fig. 1. Device design for probing ultimate plasmon confinement limits. (**A**) Graphene is encapsulated in a dielectric (few-nanometer-thick Al_2O_3 or monolayer h-BN) and covered by an array of gold rods. A gate voltage V_{BG} is applied between Si and graphene in order to control the Fermi energy of the graphene E_F. (Bottom left inset) Schematic cross section of the device. (**B** and **C**) Simulated plasmonic field magnitude profiles for metal-graphene separation *s* of 10 and 1 nm. (**D**) Simulated plasmon wavelength λ_p as a function of metal-graphene spacer *s* for the two materials used in the experiments (λ_0 = 8 μm and E_F = 0.54 eV). The vertical dashed line refers to the fundamental limit: a monolayer h-BN spacer. Colored circles correspond to the two sets of devices discussed in the main text. The dotted lines represent the model where the metal was considered as a perfect conductor in combination with the local graphene conductivity model. The dash-dotted lines represent the nonlocal graphene conductivity model (obtained from the random-phase-approximation), but still metal as a perfect conductor. The solid lines represent the model where nonlocal optical response for both metal and graphene is considered.

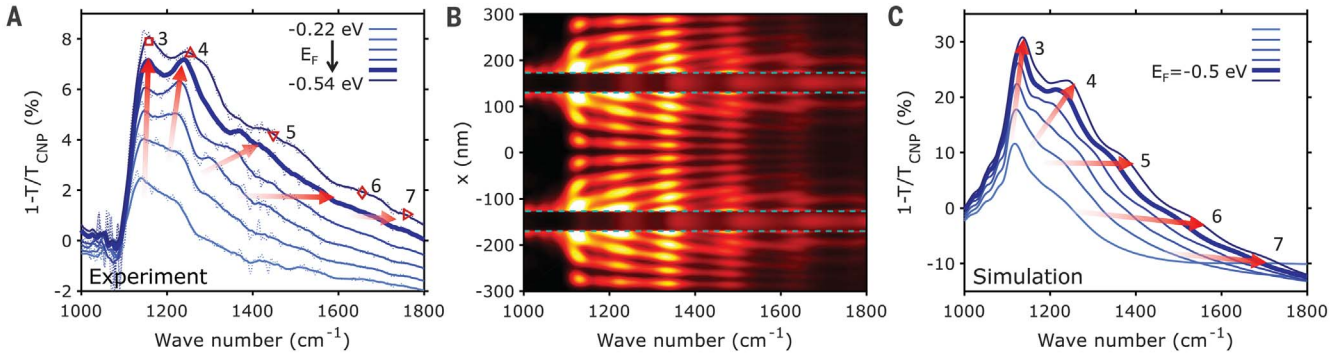

Fig. 2. Resonant excitation of 2-nm confined Fabry-Pérot SGP modes. (**A**) Gate-dependent FTIR extinction spectra referenced to the charge neutrality point (CNP) for metal rod width *w* = 256 nm, gap *g* = 44 nm, and 2-nm Al_2O_3 spacer between graphene and the metal. For increasing E_F, the resonances increase in intensity and blue shift, and high-order modes become visible. (**B**) Simulation of the electric field intensity at the graphene and along *x*, which is along the short axis of the rods, for the same device geometry as in (A), with E_F = 0.5 eV. The model considers the local response of the gold and the local response of graphene. The color scale is linear. (**C**) Simulated extinction for the device geometry as in (A), and same model as for (B).

$(1 - T/T_{CNP})$ curves were measured (Fig. 2A) for a device with continuous graphene (unpatterned), covered with 2 nm Al_2O_3 spacer (*s* = 2 nm) and metallic rods of 256 nm (*w* = 256 nm). These curves are obtained from the transmission curves *T* normalized by the transmission of undoped graphene T_{CNP} [at the charge neutrality point (CNP)] for several gate voltages (hence, Fermi energies E_F) [(*19*), section 2.2] at the same position, with light polarized perpendicular to the rod's long axis. The spectra in Fig. 2A exhibit multiple resonances, which become more pronounced and continuously blue shift with increasing Fermi energies, thus confirming their plasmonic nature. The appearance of multiple peaks demonstrates that the incoming light can resonantly couple to several higher-order plasmonic modes, in contrast to patterned graphene ribbons, as reported previously (*21*). We found up to five visible resonances that can be controlled by the spacer thickness and the metallic array geometry.

We corroborated the phenomenon by examining the simulated electric field intensity profiles at the graphene surface for the same geometry as that of the measured device (Fig. 2B) and the corresponding simulated extinction spectra (Fig. 2C). These FTDT simulations [(*19*), section 4] show a good agreement with the experiment (for *s* = 2 nm) in terms of peak shape and position by using the local optical response of graphene as well as a local metal permittivity model. The resonances can be related to Fabry-Pérot behavior of the propagating SGPs below the metal, and the resonance orders *m* can be approximated by half the number of nodes in the field profile (Fig. 2B). This observation confirms that resonances up to the seventh order are contributing to optical extinction, whereas for patterned graphene (*21*, *23*), only very weak second-order resonances have been experimentally reported. We attribute the efficient launching of these higher-order resonances to the strong dipole modes at the metal edges [(*19*), section 9], which provide the required momentum to scatter light into graphene plasmons.

To probe the physical limits of SGP confinement, we studied devices with a metal-graphene

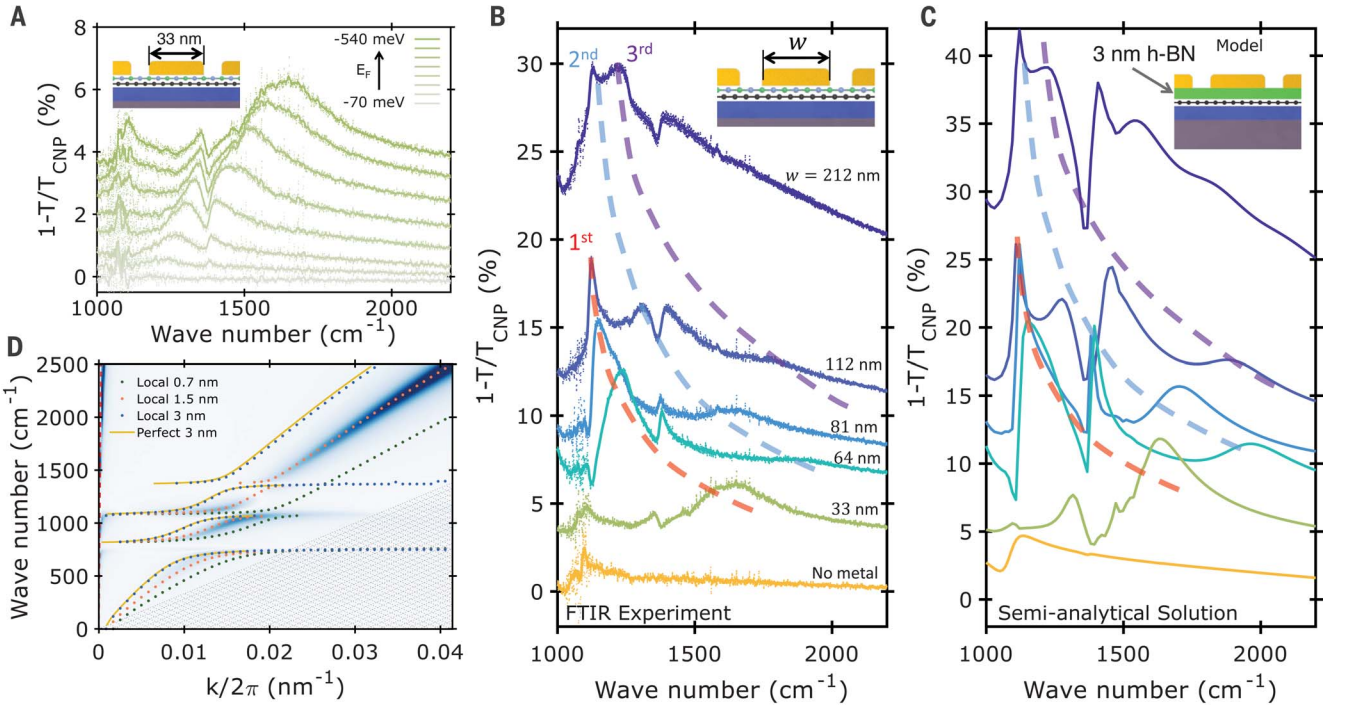

Fig. 3. Single mode and Fabry-Pérot SGP modes confined to a monolayer h-BN. (**A**) Extinction spectra for E_F ranging from 70 to 540 meV, and fixed $w \approx 33$ nm, gap $g \approx 37$ nm. (**B**) Extinction spectra for w ranging from 33 to 212 nm, and fixed $g = 38 \pm 4$ nm, $E_F = 540$ meV. Dashed lines are guides to the eye showing the evolution of each resonance with w. (Inset) Monolayer device schematic for data in (A) and (B). (**C**) Simulated extinction spectra where the nonlocal metal effects are accounted for by modeling a perfectly conducting metal but an effective thicker 3-nm h-BN spacer. (Inset) Model schematic. (**D**) Plasmon dispersion relation for a (continuous) SiO_2/graphene/h-BN/metal/air heterostructure. Dotted curves correspond to local metal response [with nonzero loss; (*19*), section 3] and are plotted for h-BN thickness of 0.7 nm (green), 1.5 nm (orange), and 3 nm (blue). The solid yellow curve corresponds to h-BN thickness of 3 nm (yellow) and modeling the metal as perfectly conducting. The blue color gradient represents the loss function of the heterostructure for 0.7-nm-thick h-BN with nonlocal metal (titanium) and nonlocal graphene response. This illustrates that accounting for nonlocality comes down to adding an extra spacer thickness of ~2 nm to a model that considers only the local metal response.

spacer with only one monolayer of chemical vapor deposition–grown h-BN of thickness ~0.7 nm (*24*, *25*). The extinction spectra were obtained for various E_F of a device with $w = 33$ nm and $g = 37$ nm (Fig. 3A). Even in this case, the SGP resonances were still visible, with high extinction values. A single plasmon peak was clearly visible and blue shifted for increasing E_F while hybridizing and anticrossing with SiO_2 and h-BN phonons. This shift with Fermi energy confirms that the extinction resonance is due to graphene plasmons.

The propagating character of the SGP modes can be assessed by further increasing w, which allows us to probe higher-order Fabry-Pérot resonances. We will show that this measurement is equivalent to changing the plasmonic cavity width w, which defines the resonant conditions. We studied the extinction of several devices with increasing w and similar gap around $g = 40$ nm and doping of $E_F = 0.54$ eV (Fig. 3B). Additional doping dependences of these devices can be found in fig. S5. The first-order resonance (Fig. 3B, red dashed line) displays hybridization with the optical phonons of its dielectric environment (as observed for plasmons in graphene nanoribbons) (*26*). We observed that when increasing w, the first-order resonance shifts to lower energies and hybridizes not only with the h-BN phonons but also with the SiO_2 phonons. More resonances appear with increasing w. For example, for $w = 64$ nm, a second-order resonance appears at 1900 cm^{-1} (Fig. 3B, blue dashed line), which also shifts for larger w and starts hybridizing when increasing w. For the largest w, the third-order (Fig. 3B, purple dashed line) and even fourth-order resonances appear for our measurement range.

The same trends are seen in the calculated spectra (Fig. 3C), obtained from a semi-analytical approach, which consists of a Fourier decomposition of the fields (for transverse magnetic modes) in each dielectric region of the system [(*19*), section 5]. In addition, for these very tightly confined optical fields, one must also take into account that the nonlocal optical response of both the metal and graphene can have appreciable effects. First of all, the in-plane momentum of the graphene plasmon is strongly enhanced by the presence of the metal and approaches $\omega/v_{F,graphene}$, where the momentum dependence of the graphene optical conductivity (nonlocal corrections to the conductivity) increases (*9*). These graphene nonlocal corrections are modeled within the framework of the random-phase-approximation (RPA) [(*19*), section 5.6]. Second, because of additional strong vertical field confinement on the order of 1 nm, the components of out-of-plane wave vectors approach $\omega/v_{F,metal}$, which is the Fermi momentum of the charge carriers in the metal (*16*). This trend can lead to additional nonlocal effects in the metal, resulting in field penetration into the metal. It is therefore relevant to quantify these effects in order to determine fundamental limits of the vertical field confinement of the propagating plasmon.

Before we discuss a more rigorous treatment of the metal nonlocal effects, we provide a qualitative picture (*27*), in which the nonlocal metal permittivity (NMP) was modeled as a dielectric shell surrounding a local metal permittivity (LMP) bulk material. Applying this model to our system, we used a perfect conductor model (with zero damping) for the bulk metal, and the thickness s of a uniform dielectric spacer was used as a fitting parameter. Simulations for this case, with an effective dielectric thickness of 3 nm (Fig. 3C), show good agreement with the experiment (Fig. 3B). Even though this result conflicts with the estimated spacer thickness (0.7 nm), the nonlocal effect can be understood by recognizing that the

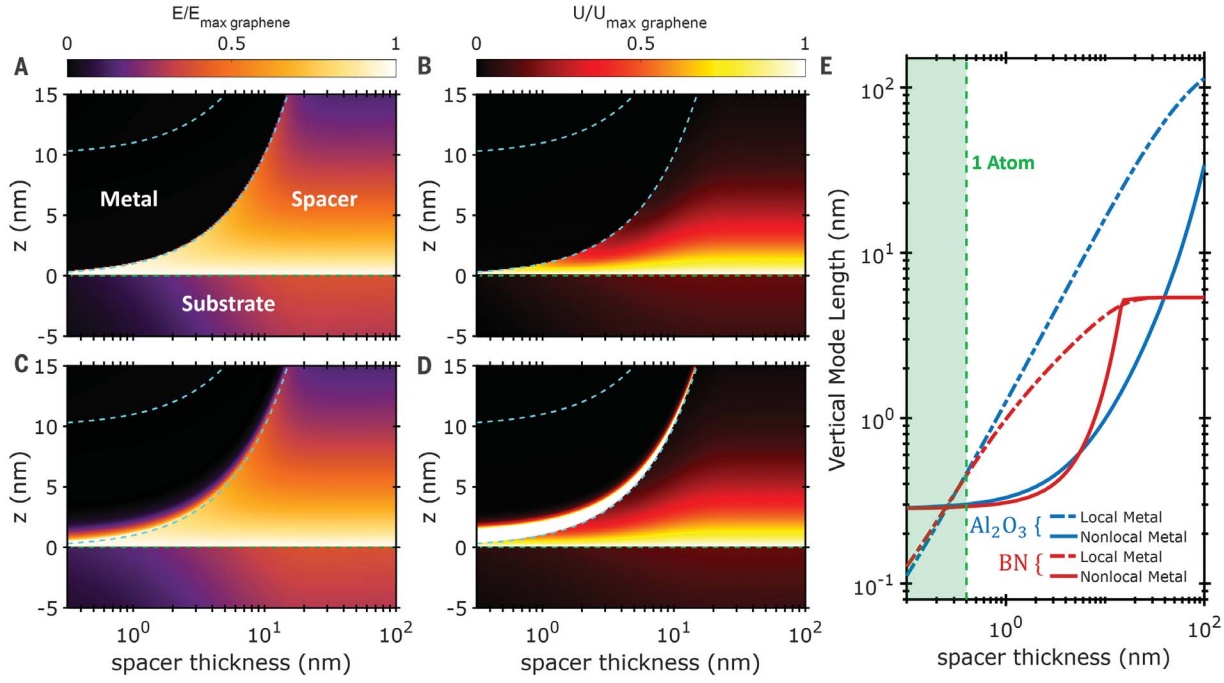

Fig. 4. Energy density and field confinement. (**A** and **C**) Electric field magnitude distribution of the plasmons associated to a continuous heterostructure of air/Ti/h-BN/graphene/SiO_2 as a function of h-BN thickness for (A) LMP model and (C) NMP model. The top and bottom metal limits are depicted by blue dashed lines, and graphene is located at $z = 0$. Normalization by the maximum electric field strictly above graphene shows the confinement and screening effects. (**B** and **D**) Same as (A) and (C), respectively, but for energy density. (**E**) Vertical field confinement for both types of dielectrics as a function of the spacer thickness for local (dash-dotted lines) and nonlocal (solid lines) metal permittivity.

electromagnetic field does penetrate more into the metal for smaller s (Fig. 4 and fig. S13), increasing the effective s.

The excited plasmon modes associated with the extinction peaks in Figs. 2 and 3 can be seen as a combination of SGPs under the metal and unscreened graphene plasmons in the gap region, with their relative contribution depending on the geometry. Nevertheless, the calculated field profiles in Fig. 1, B and C, and the scaling of the plasmon resonance peak energy with w clearly show that the electric field (associated with the plasmon modes) is mostly confined between the metal and the graphene. This confinement is also consistent with the observations that the plasmon resonances shift most substantially when varying w compared with a change of the gap g [(*19*), section 3] and that the system can be seen as a plasmonic crystal (analogous to photonic crystals) (*22*).

To further explore that a thicker dielectric in the LMP model results in nonlocal effects in the metal, the dispersion relation of the SGP modes is shown in Fig. 3D. The dispersion relation for a fully NMP model is offset to higher energies as compared with a LMP model, accounting for the proper h-BN thickness (0.7 nm) (Fig. 3D, green dotted line). Accounting for a thicker dielectric spacer used to fit our data ($s = 1.5$ nm), the dispersion curves shift down and overlap with the NMP model. Qualitatively, this is in agreement with our findings. An additional shift is expected for a periodic structure instead of a continuous one, as calculated in Fig. 3D, because of a small coupling between the modes below the rods.

We can now evaluate the ultimate limit on the plasmonic vertical field and mode volume confinement. We have calculated the electric field intensity and energy density distribution for different spacer thicknesses (Fig. 4) and considered both LMP and NMP models. We used the definitions in section 5 of (*19*), taking into account dispersion effects. Inspecting first the electric field magnitude obtained from the LMP model and normalized by the maximum of the graphene plasmon (Fig. 4, A and B), we found that most of it is confined between the graphene and the metal and that the penetration of the field inside the metal is negligible. On the other hand, considering metal nonlocal effects (NMP model) offers a more complete picture of the physics of the electrons that accumulate at the metal surface in order to screen the electromagnetic field (*18*). When the out-of-plane wave vector is increased for thinner spacers, the electrons start suffering from Pauli and electrostatic repulsion. This effect results in a saturation of the electron density and leads to field penetration into the metal as the metal screening capability is reduced (*28*). The penetration of the field into the metal becomes considerable for s below 3 nm, although the field remains maximum in the spacer region.

This nonlocal field penetration limits the vertical mode length, which is defined by the ratio of the energy density integrated over the out-of-plane coordinate z to the maximum of the field intensity in the region of the spacer (*29*, *30*)

$$L = \frac{\int u_E(z)dz}{\max u_E(z)} \quad (1)$$

The energy density distribution (Fig. 4D) peaks at the metal surface for a NMP model as a consequence of charge accumulation and the combination of high field and permittivity values, which is in contrast to the LMP (Fig. 4C). Below a certain spacer thickness, the energy density at the metal surface becomes larger than the energy density in the dielectric region near graphene. At this point, the transition of the maximum energy density from graphene to the metal dominates the vertical mode length (Fig. 4E). The out-of-plane confinement is calculated from Eq. 1 and the energy density distribution that is shown in Fig. 4E. Whereas for LMP the vertical mode length can be made arbitrarily small, the nonlocal metal behavior limits the vertical mode length to ~0.3 nm. This corresponds to a plasmonic mode confinement down to the atomic scale, as confirmed with our experiments.

These results raise the question: Why is the plasmonic mode for $s < 1$ nm, which substantially penetrates the metal (because of nonlocal response), not overdamped through Landau damping? For metals, the strongest confinement normal to the surface is limited by direct excitation of electron-hole pairs (Landau damping), which is accounted for by the nonlocal

response function (*15*). A quantitative analysis of the metallic nonlocal corrections to the dynamic response and damping through the Feibelman parameters (*18*, *31*) revealed that these effects are much stronger for ω approaching ω_p. For $\omega << \omega_p$, the imaginary part of the Feibelman parameters approaches zero as the phase space for electon-hole excitations decreases with ω. However, the real part of the Feibleman parameters does remain finite for $\omega << \omega_p$, which means that nonlocal effects persist for smaller ω, but damping contributions vanish. Thus, for our experimental conditions (with $\omega << \omega_p$), the metal nonlocal effects are relevant because the electrons in the metal cannot perfectly screen the field, but the additional damping from electronic excitations in the metal is weak.

In terms of ultimate mode volume limit, a reduction of vertical confinement reduces also the lateral propagating plasmon wavelength (Fig. 1D). Although our experiment discloses the fundamental limits of the vertical mode length of $\lambda_0/26{,}000$, it also allows us to estimate the complete mode volume confinement V_p with respect to the volume associated with the extent of the free photons $V_0 = \lambda_0^3$. If instead of an array (as in this work), a single resonant structure (for example, a metal disc on graphene, with a monolayer h-BN spacer) was built with our approach, a vertical mode length down to 0.3 nm and plasmon wavelenth $\lambda_p = \lambda_0/170$ (Fig. 1D) would be attainable, and potentially even smaller λ_p is possible with twisted bilayer graphene (*32*). Using these values (for λ_0 = 8 μm), which include the full nonlocal response for both graphene and metal, this would correspond to a mode volume of $V_p = 664\ nm^3$ and mode volume ratio $V_0/V_p \approx 10^{-9}$, which is at least two orders of magnitude smaller than reported so far with graphene nanoribbons (*20*) and sufficiently small to explore new regimes of light-matter interactions, such as the ultrastrong coupling regime.

Our results show that 2D-material heterostructures can be considered as a powerful toolbox for nanophotonics with vertical subnanometer precision. In general, patterned metals in the vicinity of van der Waals heterostructures do strongly influence the Coulomb interactions, collective excitations, and even the electronic band structure, which proves itself as an exciting platform for designing novel quantum and topological phenomena. The metallic structure can also be used as a nearby efficient gate (*7*) and provides a route to applications such as molecular sensing with even higher resolution, to enhance nonlinear effects, or to design photodetectors with plasmon-enhanced sensitivity and tunability.

REFERENCES AND NOTES

1. A. K. Geim, I. V. Grigorieva, *Nature* **499**, 419–425 (2013).
2. K. S. Novoselov, A. Mishchenko, A. Carvalho, A. H. Castro Neto, *Science* **353**, aac9439 (2016).
3. T. Low *et al*., *Nat. Mater.* **16**, 182–194 (2017).
4. D. N. Basov, M. M. Fogler, F. J. García de Abajo, *Science* **354**, aag1992 (2016).
5. A. Woessner *et al*., *Nat. Mater.* **14**, 421–425 (2015).
6. A. Principi, R. Asgari, M. Polini, *Solid State Commun.* **151**, 1627–1630 (2011).
7. V. V. Popov, *J. Infrared Millim. Terahertz Waves* **32**, 1178–1191 (2011).
8. P. Alonso-González *et al*., *Nat. Nanotechnol.* **12**, 31–35 (2017).
9. M. B. Lundeberg *et al*., *Science* **357**, 187–191 (2017).
10. M. I. Stockman, *Phys. Rev. Lett.* **93**, 137404 (2004).
11. S. I. Bozhevolnyi, V. S. Volkov, E. Devaux, T. W. Ebbesen, *Phys. Rev. Lett.* **95**, 046802 (2005).
12. R. F. Oulton, V. J. Sorger, D. A. Genov, D. F. P. Pile, X. Zhang, *Nat. Photonics* **2**, 496–500 (2008).
13. J. A. Dionne, L. A. Sweatlock, H. A. Atwater, A. Polman, *Phys. Rev. B* **73**, 035407 (2006).
14. H. T. Miyazaki, Y. Kurokawa, *Phys. Rev. Lett.* **96**, 097401 (2006).
15. J. B. Khurgin, G. Sun, in *Quantum Plasmonics*, S. Bozhevolnyi, L. Martin-Moreno, F. Garcia-Vidal, Eds. (Springer, 2016), ch. 13, pp. 303–322.
16. C. Ciracì *et al*., *Science* **337**, 1072–1074 (2012).
17. F. Benz *et al*., *Science* **354**, 726–729 (2016).
18. T. V. Teperik, P. Nordlander, J. Aizpurua, A. G. Borisov, *Phys. Rev. Lett.* **110**, 263901 (2013).
19. Materials and methods are available as supplementary materials.
20. V. W. Brar, M. S. Jang, M. Sherrott, J. J. Lopez, H. A. Atwater, *Nano Lett.* **13**, 2541–2547 (2013).
21. H. Yan *et al*., *Nat. Photonics* **7**, 394–399 (2013).
22. I.-T. Lin, C. Fan, J.-M. Liu, *IEEE J. Sel. Top. Quantum Electron.* **23**, 144–147 (2017).
23. Z. Fang *et al*., *ACS Nano* **7**, 2388–2395 (2013).
24. K. K. Kim *et al*., *Nano Lett.* **12**, 161–166 (2012).
25. J. H. Park *et al*., *ACS Nano* **8**, 8520–8528 (2014).
26. V. W. Brar *et al*., *Nano Lett.* **14**, 3876–3880 (2014).
27. Y. Luo, A. I. Fernandez-Dominguez, A. Wiener, S. A. Maier, J. B. Pendry, *Phys. Rev. Lett.* **111**, 1 (2013).
28. C. David, F. J. García de Abajo, *ACS Nano* **8**, 9558–9566 (2014).
29. R. Ruppin, *Phys. Lett. A* **299**, 309–312 (2002).
30. S. A. Maier, *Opt. Express* **14**, 1957–1964 (2006).
31. T. Christensen, W. Yan, A. P. Jauho, M. Soljačić, N. A. Mortensen, *Phys. Rev. Lett.* **118**, 157402 (2017).
32. T. Stauber, P. San-Jose, L. Brey, *New J. Phys.* **15**, 113050 (2013).

ACKNOWLEDGMENTS

The authors thank G. Konstantatos and V. Pruneri for the intensive use of their respective FTIRs and are grateful for very insightful discussions with M. Polini, T. Christensen, A. Mortenson, and J. Aizpurua on nonlocal effects and with A. Woessner on simulation and modeling of graphene acoustic plasmons modes. **Funding:** We acknowledge financial support from the Spanish Ministry of Economy and Competitiveness, through the Severo Ochoa Programme for Centres of Excellence in R&D (grant SEV-2015-0522), and support by Fundacio Cellex Barcelona, the Mineco grants Ramon y Cajal (grant RYC-2012-12281), Plan Nacional (grants FIS2013-47161-P and FIS2014-59639-JIN), and the government of Catalonia through the SGR grant (2014-SGR-1535). Furthermore, the research leading to these results has received funding from the European Union H2020 Programme under grant agreement 604391 Graphene Flagship, the European Research Council starting grant (307806, CarbonLight), and project GRASP (FP7-ICT-2013-613024-GRASP). D.A.I. acknowledges the FPI grant BES-2014-068504. N.M.R.P. and E.J.C.D acknowledge support from the Portuguese Foundation for Science and Technology (FCT) in the framework of the Strategic Financing UID/FIS/04650/2013. This work was supported in part by the Center for Excitonics, an Energy Frontier Research Center funded by the U.S. Department of Energy, Office of Science, Office of Basic Energy Sciences, under award DE-SC0001088, and the Army Research Office (grant 16112776). J.-Y.H. and J.K. acknowledge support from the U.S. Air Force Office of Scientific Research Foldable and Adaptive 2D Electronics Multidisciplinary University Research Initiative, grant FA9550-15-1-0514. **Author contributions:** F.H.L.K, D.A.I., and S.N. conceived the idea; E.J.C.D and N.M.R.P. developed the analytical model; S.N., C.P., J.O., D.K.E., and D.A.I. fabricated the devices; S.N., R.P., and D.A.I. performed measurements; D.A.I., M.B.L., I.E., and S.N. performed data analysis; J.-Y.H. and J.K. provided h-BN; D.A.I., S.N., E.J.C.D., N.M.R.P, I.E., D.K.E., and F.H.L.K wrote the manuscript; and D.R.E. and F.H.L.K. supervised the project. **Competing interests:** None of the authors have competing interests. **Data and materials availability:** All data needed to evaluate the conclusions in the paper are present in the paper and/or the supplementary materials.

SUPPLEMENTARY MATERIALS

www.sciencemag.org/content/360/6386/291/suppl/DC1
Materials and Methods
Supplementary Text
Figs. S1 to S17
References (*33*–*47*)

25 December 2017; accepted 26 February 2018
10.1126/science.aar8438

Science

Probing the ultimate plasmon confinement limits with a van der Waals heterostructure

David Alcaraz Iranzo, Sébastien Nanot, Eduardo J. C. Dias, Itai Epstein, Cheng Peng, Dmitri K. Efetov, Mark B. Lundeberg, Romain Parret, Johann Osmond, Jin-Yong Hong, Jing Kong, Dirk R. Englund, Nuno M. R. Peres and Frank H. L. Koppens

Science **360** (6386), 291-295.
DOI: 10.1126/science.aar8438

Light confined to a single atomic layer

The development of nanophotonic technology is reliant on the ability to confine light to spatial dimensions much less than the wavelength of the light itself. Typically, however, in metal plasmonic approaches, there is a trade-off between confinement and losses. Alcaraz Iranzo *et al.* fabricated heterostructures comprising monolayers of graphene and hexagonal boron nitride (hBN) and an array of metallic rods. The light was confined vertically (as propagating plasmons) between the metal and the graphene, even when the insulating hBN spacer was just a single monolayer. Such heterostructures should provide a powerful and versatile platform for nanophotonics.

Science, this issue p. 291